CHAPTER- 7

EFFECT OF SYNTHESIS TECHNIQES ON Sr DOPED LANTHANUM FERRITE

Uma Sharma, Jay N. Mishra, Vani Pawar, Prabhakar Singh, "To examine the effect of synthesis techniques on the physical and electrochemical properties of Lanthanum Strontium Ferrite (LSF)", (Under Preparation).

CHAPTER 7: Effect of synthesis techniques on Sr doped Lanthanum Ferrite (LSF)

7.1 Introduction

In chapter 6, it has been observed that reducing the size of the A-site substituted $LaFeO_3$ through hydrothermal method will affect the electrochemical behavior.

In this work, we compare the behavior of the formed nanoparticle with the bulk LSF investigated in the previous chapter. This chapter presents the investigation of Strontium (Sr) at A-site doped $LaFeO_3$, synthesized through the hydrothermal method. The formation of nanoparticles confirmed through the TEM images. The structural study of samples was carried out and crystallite size was estimated with the help of Debye-Scherrer's formula (Equation 2.2). Rietveld refinement was performed for the prepared nano-particle. Electrochemical impedance measurements were performed, and the ionic conductivity of the sample was studied.

We termed the $LaSrFeO_3$ synthesized via hydrothermal as nano-LSF (N-LSF), while the previously synthesized LSF through solid-state reaction method is referred as bulk-LSF (B-LSF).

7.2 Experimental Procedure

Preparation of LSFO Nanocrystalline Particles: LSF nanoparticles were prepared using the hydrothermal method. Firstly, lanthanum nitrate hexahydrate, strontium nitrate, and iron nitrate nonahydrate were weighted in stoichiometric proportions. These were dissolved in deionized water by a magnetic stirrer. Subsequently, when the metal salts were utterly

dissolved in the solution, then 10 mL of ethylene glycol and aqueous ammonia were added to maintain the pH value to 12. This solution was ultrasonicated for 30 min, then transferred into a 100 mL Teflon autoclave and kept at 180 ℃ for 24 h. After cooling at room temperature, formed products were washed with deionized/distilled water and ethylene glycol several times. These were dried at 80 ℃ for 12 h and then ground and calcined at 1000 ℃ for 4 h in muffle furnace to obtain dry powders.

Details of the solid-state reaction route synthesis process has been already discussed in previous chapters.

Room-temperature X-ray diffraction patterns of the studied sample were recorded with the Cu-Kα radiation using X-ray Diffractometer in the 2θ range from 20°-70° at the scan rate of 5°/min and step size of 0.01°. Microstructural characterization was done by scanning electron microscopy. The X-ray photoelectron spectrum was recorded using Mg target at room temperature and under 10^{-6} Pa pressure. For the electrochemical studies of the samples cyclic voltammetry has been performed with a three-electrode electrochemical cell.

7.3 Results and Discussion

7.3.1 Structural Studies

Fig 7.1 shows the X-ray diffraction patterns of LSF in bulk and nano form, respectively. All the diffraction peak positions of nano LSF are in agreement with the Bulk LSF. Rietveld refinement of both, B-LSF and N-LSF confirms the Pbnm (Space group No 62) symmetry.

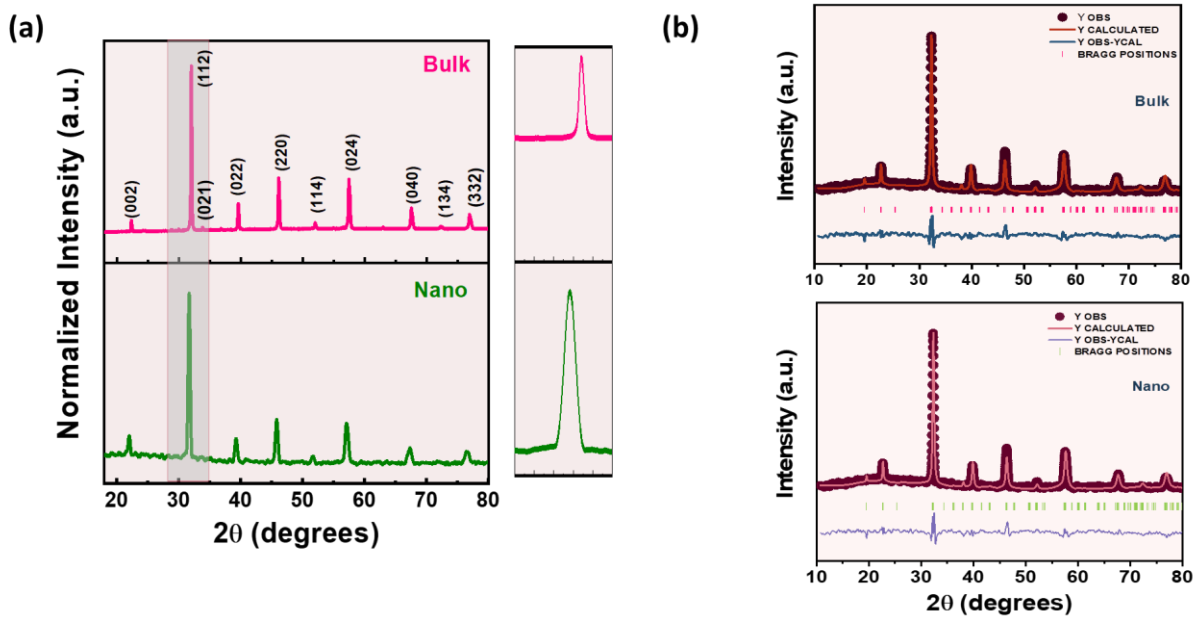

Figure 7.1 (a) X-ray diffraction patterns of B-LSF and N-LSF **(b)** Reitveld refinement of both B-LSF and N-LSF.

The crystallite size and microstrain estimated for both the samples based on Scherrer's equation given in chapter 2 (eq. 2.2) using full width at half maximum of the XRD pattern (refer to W-H plot Fig. 7.2)[212]. The estimated crystallite size value is 21.23 nm and 4.05 nm for the B-LSF and N-LSF, respectively. Also, a broadening of peaks observed in the N-LSF which also suggest that crystallite size is reduced[213]. A higher microstrain is observed in N-LSF compared to B-LSF[214]. These outcomes indicate the formation of the nanoparticles.

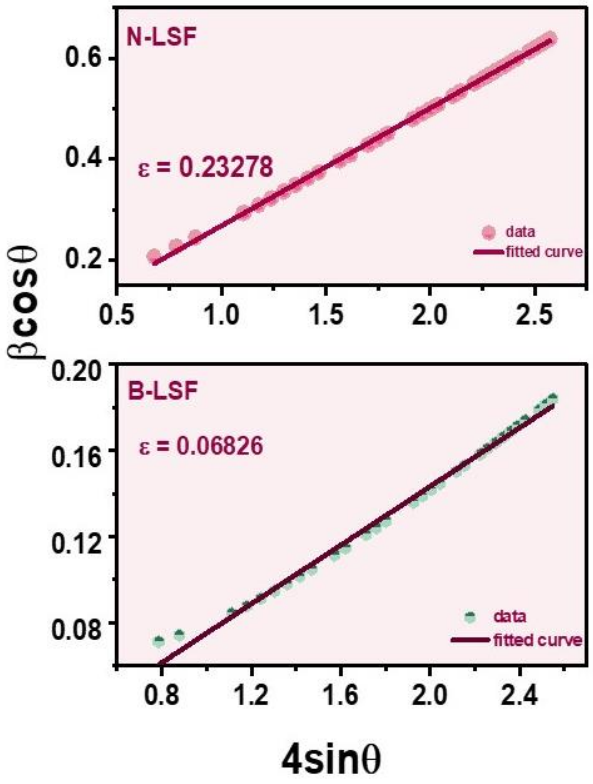

Figure 7.2 W-H plot of of B-LSF and N-LSF and estimated value of micro strain.

7.3.2 Surface Morphology and Particle Size

Figure 7.3(a)-(b) shows the SEM micrographs of the LSF formed using the Solid-state reaction method and the hydrothermal method, denoted as B-LSF and N-LSF, respectively. An apparent change in morphology was observed with synthesis; in bulk LSF, a rhombohderal grains are observed, but in the case of nano-formed LSF, a reduction in grain size was observed.

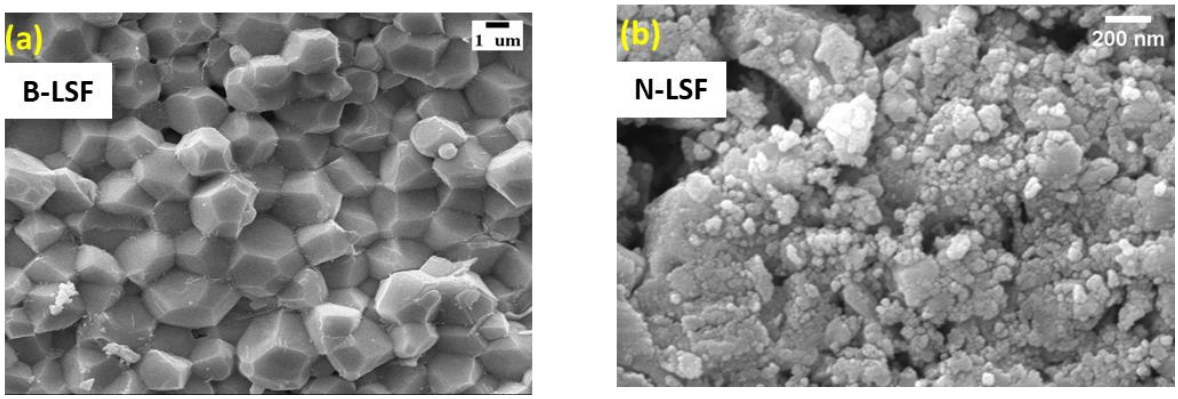

Figure 7.3 (a)-(b) SEM micrograph of Bulk LSF and Nano LSF particles.

The TEM analysis of the nano LSF is shown in Fig. 7.4(a) and was used to determine the detailed structural characterization. The morphology indicates the presence of dispersed tiny particles, suggesting the formation of nanoparticles given that their size falls within the nanometer range. The particle size, calculated from the TEM micrographs, is 35.17 nm, which is in good agreement with the estimated value from the instrument, corroborating these findings (refer to Fig. 7.4).

The SAED pattern also observed (refer to Fig. 7.4(c)) for N-LSF provides information about the nature of the phase present in the composition. It suggests that the N-LSF sample exhibits a polycrystalline nature with some different rings, indicating the preparation of a single-phase composition. These rings correspond to various planes within the structure[141][215].

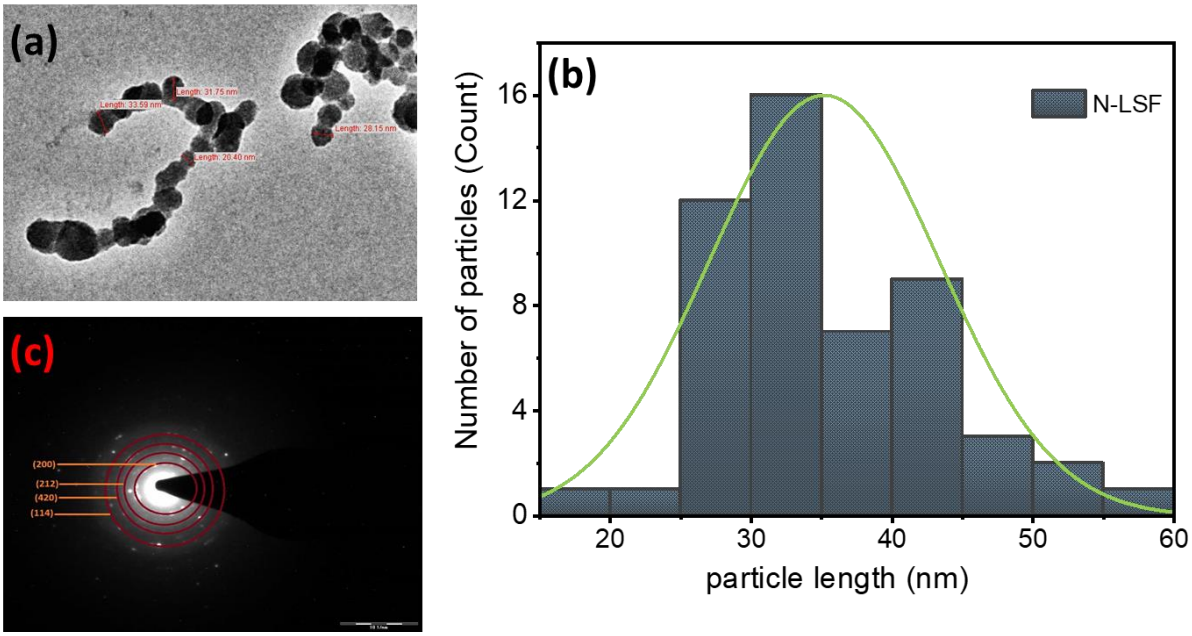

Figure 7.4 (a) TEM images of Nano-LSF confirms the formation of nanoparticle **(b)** TEM micrographs with particle size distribution **(c)** SAED pattern.

7.3.3 Electrochemical Analysis

Electrochemical responses of both the samples in aqueous 1M Na_2SO_4 solution at room temperature are shown in Fig 7.5. The cyclic voltammogram depicted in the figure was studied in the sweep potential range of -1.5 V to -1.5 V and scan rate of 25, 50, 100, 150, 200 & 250 mV/s. It was observed that the value of current increases with the increase in the scan rate in both the cases. The area of the curve also increases with the increase in the sweep rate. The current density was higher for B-LSF as compared to N-LSF for the same scan rate. For B-LSF, significant oxidation and reduction peaks are observed, whereas, for N-LSF, reduction peak are prominent. It suggests that the redox response of B-LSF is more than N-LSF [216].

Since, there is higher current density observed in the case of B-LSF in comparison to N-LSF, it suggests that N-LSF might possesses capacitive property.

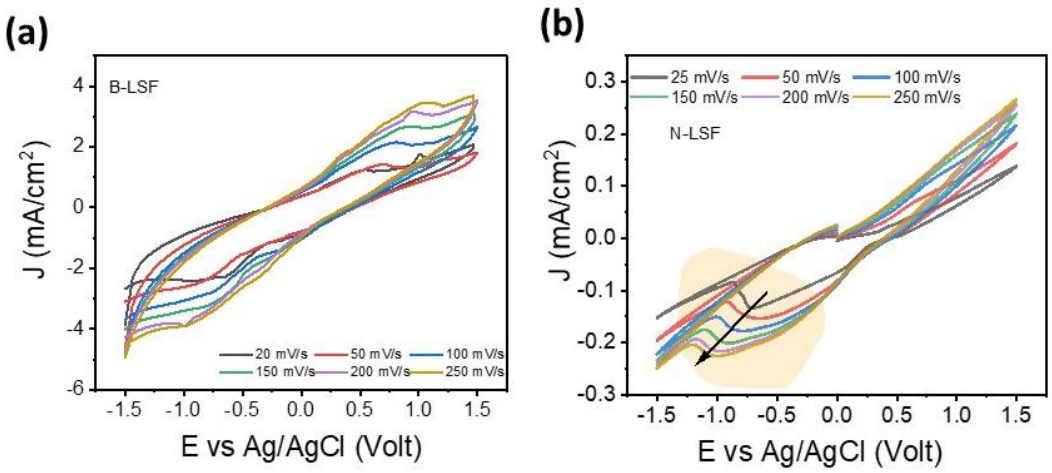

Figure 7.5 Cyclic Voltammogram curve of **(a)** B-LSF **(b)** N-LSF with various scan rate.

For that, the specific capacitance (C) calculated from the CV graph of both the sample, using equation-

$$C = \int \frac{I(v)\, dv}{mv\nabla V} \tag{7.1}$$

where, $\int I(v)\, dv$ is area under the curve, m represents the mass of the electrode samples before the CV performed, v is the scan rate in V/s, ∇V is the potential window used during the measurement[217].

The Fig. 7.6 shows the variation of specific capacitance with scan rate for both B-LSF and N-LSF. The obtained maximum capacitance value is 800 mF/g for N-LSF which is ten times higher the value obtained through B-LSF i.e., 60 mF/g. This high capacitance in N-LSF is mainly attributed to its morphology. These electrochemical results suggest that N-LSF makes it suitable for energy storage applications.

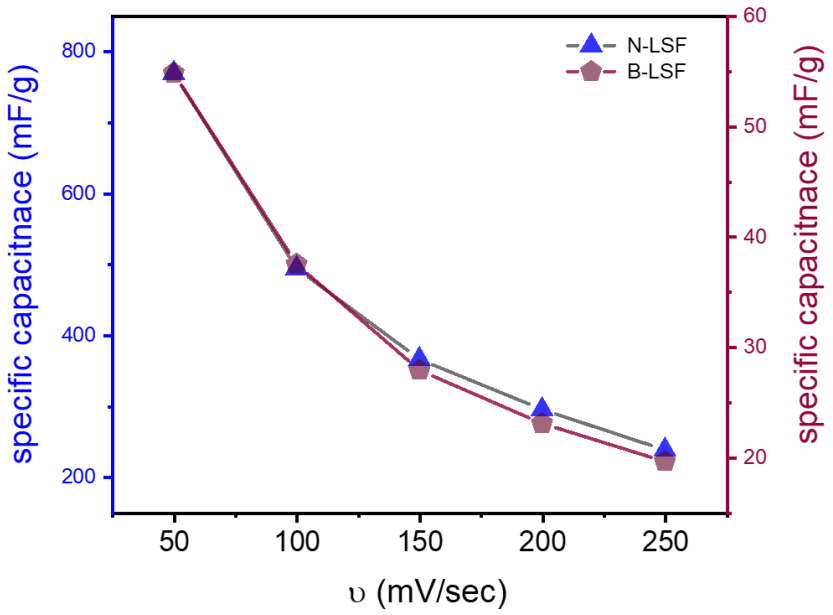

Figure 7.6 Specific capacitance at different scan rate for B-LSF and N-LSF sample.

Figure 7.7 shows the chronoamperometry plot of B-LSF and N-LSF sample at 1.5 V. Chronoamperometry measurement of the samples was recorded to examine the stability and the transient decay. It was performed at a constant potential of 1.5 V for 4000 sec and the value of current density is 0.25 A/cm^2 after the 100th second (s) of growth for the B-LSF and 0.22 mA/cm^2 after the 200th second (s) of growth for N-LSF (refer to inset of Fig. 7.7). This constant current density suggest the stable and efficient electrical conduction in both the samples.

The kinetics of charge transfer can easily be determined with the help of power law dependence of current response on the scan rate (Equation 4.8). This is confirmed by the log-log plot of scan rate and peak current density (Fig. 7.8). The estimated slope values are 0.32 for B-LSF and 0.27 for N-LSF signifies the adsorption mechanism or the surface controlled process in both the cases[186].

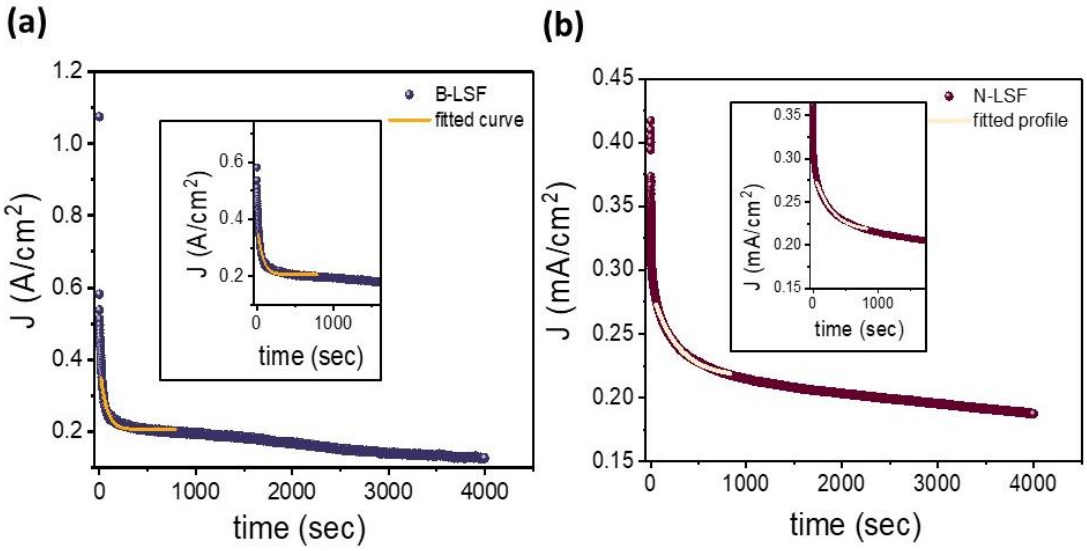

Figure 7.7 Specific capacitance at different scan rate for B-LSF and N-LSF sample.

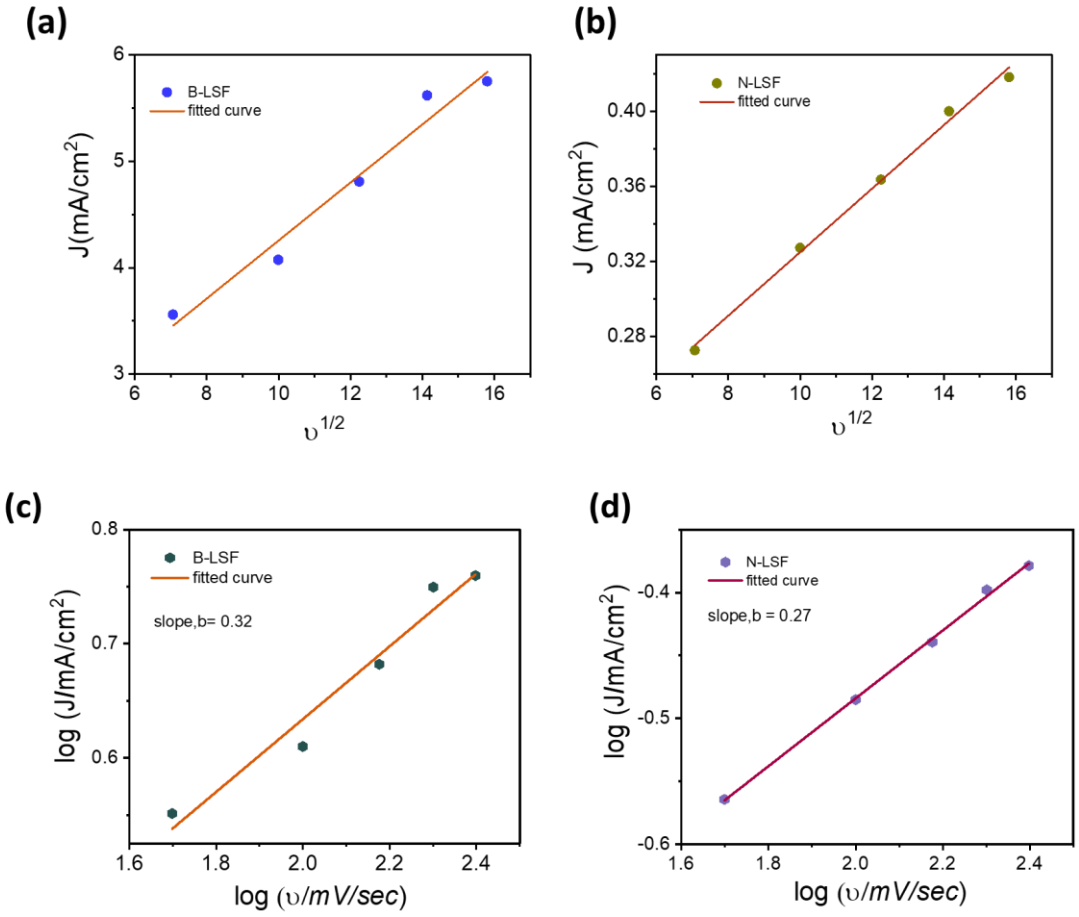

Figure 7.8 Variation of current density with $v^{1/2}$ in **(a-b)** and **(c-d)** are log-log plot of current density and v.

7.4 Conclusion

This chapter concludes the structural, morphological, and electrochemical behavior of the sample LSF prepared via different synthesis methods, i.e., Solid-State Reaction (SSR) and Hydrothermal method. The phase formation was studied via the X-ray diffraction method, and refinement was performed on both the samples, i.e., B-LSF and N-LSF. The particle size was estimated through the W-H plot. B-LSF is in micrometer and the N-LSF is in micrometer, which suggests the formation of the nanoparticle. The TEM morphology was performed to confirm the formation of nanoparticles. SEM studied comparative analysis of the morphology of B-LSF and N-LSF. The electrochemical behavior of the samples was studied with the help of cyclic voltammetry. Here, the current density is higher in the case of B-LSF compared to N-LSF. The B-LSF was adequately involved in the redox activity, whereas for N-LSF, only reduction properties are favorable. That is why the specific capacitance of both samples was estimated, and ten times higher specific capacitance (mF/g) was observed in the case of N-LSF. The calculated transient time decay value is consistent with the capacitive properties. The chronoamperometry stability test was observed for 4000 s, and both samples were stable for that period.